ARTICLE   OPEN

Scalable spin–photon entanglement by time-to-polarization conversion

Rui Vasconcelos[1,3], Sarah Reisenbauer[1,2,3], Cameron Salter[1,3], Georg Wachter[1,2], Daniel Wirtitsch[1,2], Jörg Schmiedmayer [ID][2], Philip Walther [ID][1] and Michael Trupke [ID][1,2]*

The realization of quantum networks and quantum computers relies on the scalable generation of entanglement, for which spin-photon interfaces are strong candidates. Current proposals to produce entangled-photon states with such platforms place stringent requirements on the physical properties of the photon emitters, limiting the range and performance of suitable physical systems. We propose a scalable protocol, which significantly reduces the constraints on the emitter. We use only a single optical transition and an asymmetric polarizing interferometer. This device converts the entanglement from the experimentally robust time basis via a path degree of freedom into a polarization basis, where quantum logic operations can be performed. The fundamental unit of the proposed protocol is realized experimentally in this work, using a nitrogen-vacancy center in diamond. This classically assisted protocol greatly widens the set of physical systems suited for scalable entangled-photon generation and enables performance enhancement of existing platforms.

INTRODUCTION

The generation of entangled-photon states is of central importance in linear optical quantum computing (LOQC)[1,2] and optical quantum communication,[3,4] and has potential applications in quantum sensing and metrology.[5] Currently, entangled-photon sources rely mostly on spontaneous parametric down-conversion, which is robust and offers high purity, but is limited by intrinsically probabilistic entanglement generation.[6] For most applications in quantum technology, large entangled states are necessary in order to reach performance levels which exceed those of classical devices. The generation of such states therefore remains an outstanding challenge.

Cluster states are particularly desirable resources as they enable measurement-based quantum computation and have an in-built resilience to noise and loss.[7–9] Spin-based protocols have been developed for the generation of entangled-photon strings, the most prominent of these being the "cluster-state machine gun" (CSMG) of Lindner and Rudolph.[10] This protocol is appealingly simple and robust, and can be scaled to higher-dimensional cluster states using multiple spins.[11,12] Its requirements are however quite stringent. Ideally, it necessitates two orthogonally polarized, energy-degenerate optical transitions with negligible cross-decay terms (see Fig. 1a). A first demonstration of the CSMG protocol with quantum dots was shown by Schwartz et al.[13], where the length of the cluster-state was limited to three photons due to the short lifetime of the qubit.

Here, we employ a nitrogen-vacancy (NV) defect in diamond, which is known for its excellent quantum coherence properties, and is therefore a promising candidate for quantum technology.[14–16] As a CSMG source, however, it presents several drawbacks. In particular, the optical transition energies connecting different spin states require careful tuning into resonance while maintaining negligible state mixing, and several of its excited-state levels can decay to multiple ground states and have a strong decay channel into a long-lived metastable state[17] (see Fig. 1b, c).

It is therefore challenging to adhere to the requirements of the original CSMG scheme.[18]

Instead, in this work we develop and demonstrate an alternative, scalable scheme based on time-to-polarization conversion (TPC). Its main advantage is that it requires the use of just one optical transition (Fig. 2). Therefore, the most favorable spin properties of the strongest transition available can be used, and tuning of energy levels is no longer required. With these simplifications, it is applicable to a large variety of emitters.[19,20]

RESULTS

Scheme

Briefly, our protocol starts with an equal spin superposition between the $m_s = 0$ and $m_s = -1$ optical ground states. Upon excitation, the emitter produces a photon with 50% probability, which is stored in a H-polarized channel. During the storage time the superposition of the spin is inverted by a π-rotation. A second excitation pulse can then launch a photon, again with 50% probability, into a V-polarized channel. The sequence therefore generates a single photon in a superposition of polarizations. At this stage, it is however not possible to verify entanglement on the spin-photon state as the initial spin state is revealed directly by the photon's position. The path information, and with it the emission time information, is therefore erased by matching the delay time between excitation pulses to the storage time of the H-arm. After the TPC process, the time-separated wavepackets merge into a single polarization qubit entangled with the NV center spin. The procedure can be iterated to generate a string of entangled photons. Altogether, the single optical transition and the photonic routing elements act as the ideal CSMG four-level system.

In more detail, the experimental sequence used to demonstrate the method unfolds in three steps: preparation, entanglement generation, and tomography (Fig. 3).

[1]Faculty of Physics, University of Vienna, VCQ, Boltzmanngasse 5, 1090 Vienna, Austria. [2]Institute for Atomic and Subatomic Physics, Vienna University of Technology, VCQ, Stadionallee 2, 1020 Vienna, Austria. [3]These authors contributed equally: Rui Vasconcelos, Sarah Reisenbauer, Cameron Salter. *email: michael.trupke@univie.ac.at
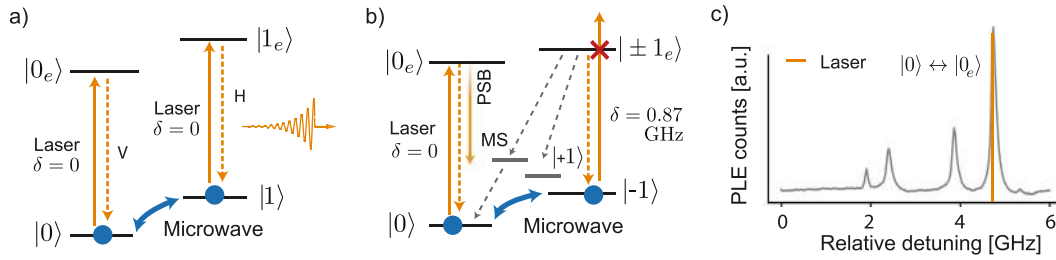
Fig. 1 Physical requirements for the cluster-state machine gun protocol. a Ideal level scheme for the protocol of Lindner and Rudolph. Simultaneous excitation of two energy-degenerate transitions creates photons of orthogonal polarizations. Starting the cycle in an equal superposition of the states $|0\rangle$ and $|1\rangle$ creates a spin-photon entangled state of the type $(|0, V\rangle + e^{i\phi}|1, H\rangle)/\sqrt{2}$ in the first iteration. **b** Simplified level scheme corresponding to the optical NV transitions. The emitter does not present the required energy-degenerate transitions with orthogonal photon polarization and undesired decay channels occur, particularly from the level $|\pm 1_e\rangle$, which can non-radiatively decay to the metastable state (MS). Radiative decay occurs via the zero-phonon line (ZPL), where spin–photon entanglement can be generated, and through the phonon-side band (PSB), which is used for spin state readout. **c** Photoluminescence excitation spectrum of the NV center used herein. The working transition ($|0\rangle \leftrightarrow |0_e\rangle$) is far-detuned (by 0.87 GHz in this experiment) from other transitions, ensuring negligible cross-excitation.
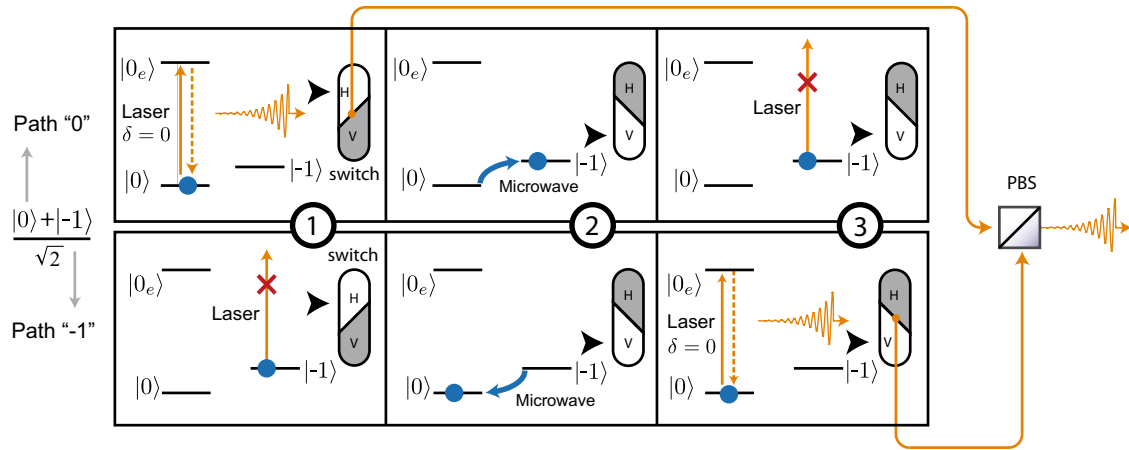

Fig. 2 Entangling scheme with time-to-polarization conversion. The ground states $|0\rangle$ and $|-1\rangle$ constitute the matter qubit. The laser is resonant with the $|0\rangle \leftrightarrow |0_e\rangle$ transition and far-detuned from other transitions, ensuring negligible cross-excitation. Path "0" ("−1") display the evolution for initialization of the spin in the state $|0\rangle$ ($|-1\rangle$), as the entangling sequence is applied to the initial spin superposition $(|0\rangle - |-1\rangle)/\sqrt{2}$. In panel ①, a laser excitation leads to the generation of a photon in path "0", which is guided via a switch into a channel that rotates the polarization to an horizontal orientation. No photon is generated in path "−1" since no resonant transition is available from the state $|-1\rangle$. In panel ②, the spin state is inverted in both paths by a microwave π-pulse and the classical optical routing is switched to a vertically polarized channel. In panel ③, a further excitation cycle is triggered with another laser pulse. Owing to the route switching, this excitation results in the generation of a vertically polarized photon in the evolution path "−1". This time, no photon is generated in path $|0\rangle$. Although the photon is emitted with the same polarization in both evolution paths "0" and "−1", the classical photonic routing and polarization elements enable the entanglement of the spin with the photon polarization. The path information is erased with a polarizing beam splitter (PBS) where the possible photon trajectories are overlapped, resulting again in the desired entangled state of the type $(|0, V\rangle + e^{i\phi}|1, H\rangle)/\sqrt{2}$ (see text).

Preparation. The experimental cycle (Fig. 3b) starts by initializing the NV charge state, through ionization into NV⁻, with a green laser pulse. The electronic and nuclear (^{14}N nucleus of the NV center) spins are then initialized by iteratively flipping undesired spin populations using resonant optical pumping (see Supplementary Information), preparing them in the $m_s = -1$, $m_I = 0$ state. The electron spin subspace $\{|0\rangle, |-1\rangle\}$ constitutes the matter qubit of the protocol. Initialization of the nuclear spin is applied to reduce dephasing and to maximize microwave transfer fidelity. We obtain a qubit initialization fidelity of $97.9 \pm 1.6\%$ and a nuclear polarization, within the $m_s = -1$ manifold, of $83.8 \pm 1.9\%$.

Entanglement generation. After initialization of the electron spin into $|-1\rangle$, a rotation with a microwave pulse $R_y(\pi/2)$ brings the electron into a superposition $\psi_0 = (|-1\rangle - |0\rangle)/\sqrt{2}$. An optical $|0\rangle \rightarrow |0\rangle_e$ π-pulse (a_1) using a resonantly tuned laser then leads to

the emission of a photon, conditional upon the state of the electron spin, resulting in the state $\psi(a_1) = (|-1\rangle|0_{a1}\rangle - |0\rangle|H_{a1}\rangle)/\sqrt{2}$. The ket $|H_{a1}\rangle$ ($|0_{a1}\rangle$) denotes an horizontally polarized photon (no photon) created by the pulse a_1. This photon is stored for 262 ns in the long arm of the fiber interferometer (Fig. 3a). Meanwhile, a microwave π-pulse rotates the spin to the orthogonal state, $(|0\rangle|0_{a1}\rangle + |-1\rangle|H_{a1}\rangle)/\sqrt{2}$, followed by a second optical excitation (a_2), the emission of which is vertically polarized in the TPC apparatus, resulting in the entangled state $\psi(a_2) = (|0\rangle|V_{a2}\rangle + e^{i\phi}|-1\rangle|H_{a1}\rangle)/\sqrt{(2)}$, with the interferometer phase ϕ (see Methods).

We can therefore realize a circuit analogous to the building block of the CSMG protocol by selecting the appropriate phase ϕ of the interferometer: repetition of the entanglement generation step on the existing spin superposition leads to the addition of further photonic qubits to the entangled state (see Supplementary
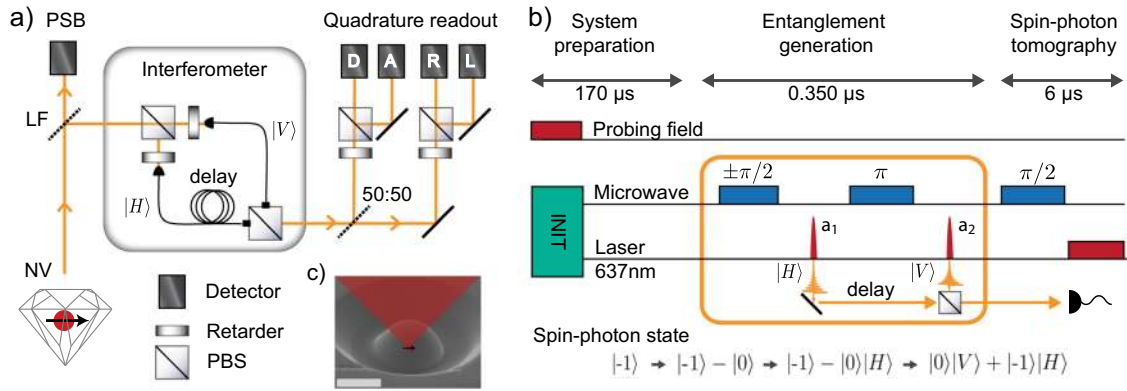
Fig. 3 Overview of the experiment. a Core elements of the photon collection path. A laser line filter (LF) separates the phonon-side band (PSB) photons from the zero-phonon line (ZPL) fluorescence path, where the spin–photon entanglement is detected. The TPC process is passively executed by the unbalanced interferometer, which consists of two polarization-maintaining single-mode fibers with a propagation time difference of 262 ns, mapping the wavepacket from the first (second) excitation/emission cycle into H (V) polarization and overlapping the two wavepackets at the output, where transmitted photons are monitored in quadrature, D/A and R/L. **b** Experimental sequence to generate polarization-based spin–photon entanglement by time-to-polarization qubit conversion (TPC). The rectangle highlights the entangling operations, which can be iterated at will to scale the output to a multiphoton entangled state. The probing field is used to measure the phase of the interferometer. The microwave operations are rotations around the spin's y-axis. Events and simplified states are shown on a time axis. **c** Electron microscope image of a solid-immersion lens milled into diamond, red overlay indicates NV emission cone. The white scale bar is 10 μm.

Information). The correct routing of the photons is probabilistic here, and is heralded by the time of arrival, but can be made deterministic with an active switch.

Tomography. On the photonic side, the passive TPC scheme enables direct projection onto both the equatorial basis (D/A and R/L) in the path-erasing events, and onto the polar basis (H/V) by selecting path-revealing events (see Methods and Supplementary Information). The D/A and R/L ports perform a projective measurement on the photon, dependent on the interferometer phase, onto the states: $|\phi^{\pm}\rangle = |H\rangle \pm e^{i\phi}|V\rangle$ and $|\phi^{\pm}_{\pi/4}\rangle = |H\rangle \pm e^{i(\phi+\pi/4)}|V\rangle$, respectively. The electron spin readout relies on the rotation of the spin state through a $R_y(\theta)$-pulse and a final 5 μs laser pulse (Fig. 3b).

We experimentally demonstrate the process using a NV center in an artificial diamond created by chemical vapor deposition. A microlens (Fig. 3c) is machined over a pre-allocated NV center by focused-ion-beam milling for improved photon collection efficiency. We manipulate the spin using a microwave field radiated from two bond wires. The diamond is cooled to ~4.5 K in a closed-cycle cryostat and photons are collected through a window using a microscope objective.

Experimental realization

The fundamental unit of the proposed protocol is experimentally demonstrated by performing partial tomography on the resulting spin-photon system and quantifying the respective entanglement. The resulting measured correlations in the $\sigma_z \otimes \sigma_z$ basis are represented in Fig. 4a, with a correlation value of $C_{zz} = \langle \sigma_z \otimes \sigma_z \rangle = (83.7 \pm 1.6)\%$.

To extract the $C_{xx} = \langle \sigma_x \otimes \sigma_x \rangle$ correlations, spin–photon entanglement is generated for two different initial spin superposition states $\psi_- = (|{-1}\rangle - |0\rangle)/\sqrt{2}$ and $\psi_+ = (|{-1}\rangle + |0\rangle)/\sqrt{2}$, corresponding to the spin measurement projection states $|\pm x\rangle$. Following established procedure,[21] we now observe the spin-photon correlations by measuring their dependence on the interferometer phase, ϕ. The measured photon entangling events, on average 25 per hour, in the quadrature ports (D, A, R, and L) are sorted according to ϕ at the time of detection and combined taking into account each port's phase offset. Figure 4b shows the conditional probability of projecting the spin state onto $|+x\rangle$ and

$|{-x}\rangle$, given the projection of a photon onto an equatorial state $|\phi\rangle = |H\rangle + e^{i\phi}|V\rangle$. The resulting curves correspond to a correlation $C_{xx} = (40.7 \pm 2.9)\%$, showing the entanglement signature expected for the ψ^+ Bell-state (as opposed to $C_{xx} = 0$ for a statistical mixture). In order to probe the quality of our source directly, the presented results have an accurately calibrated measure of the background light present in our ZPL detection window deducted (see Supplementary Information). The limiting factors contributing to the departure from the ideal state generation are discussed quantitatively in the Supplementary Information, with good agreement between theoretical estimate and measured correlations.

From the retrieved correlations, we estimate a lower bound on the entanglement fidelity with respect to the ideal Bell-state, $|\psi^+\rangle$, of $F \geq 64.7 \pm 1.3\%$ and a raw $F \geq (56.0 \pm 0.9)\%$, including background. This value is significantly above the bound for a classical state ($F \leq 50\%$), thereby demonstrating the entanglement in our spin-photon protocol, by over 11 standard deviations (over six without background subtraction). The fidelity is currently limited by a variety of imperfections (such as spin mixing in the excited-state manifold and imperfect spin readout), which can be minimized by improvements to the set-up and system (see Supplementary Information).

DISCUSSION

The TPC entanglement generation and conversion protocol proposed and demonstrated in this work points at the underlying concept of how the imperfections of a quantum system (NV system) can be counteracted by the role of a classical counterpart (interferometer). Specifically, the TPC technique relaxes many of the requirements placed on the emitter and broadens the range of systems for which such entanglement generation schemes are possible.

The experimental apparatus used in the demonstration of the protocol is currently limited to two-particle entanglement, owing to the low-photon collection efficiency, strong decay into the PSB, and long initialization cycles. The fidelity is furthermore limited by undesired transitions from the excited state. These shortcomings have known solutions: the emission and collection of ZPL photons from the optical transition can be drastically improved using an optical resonator,[22] and fast initialization is achievable with an
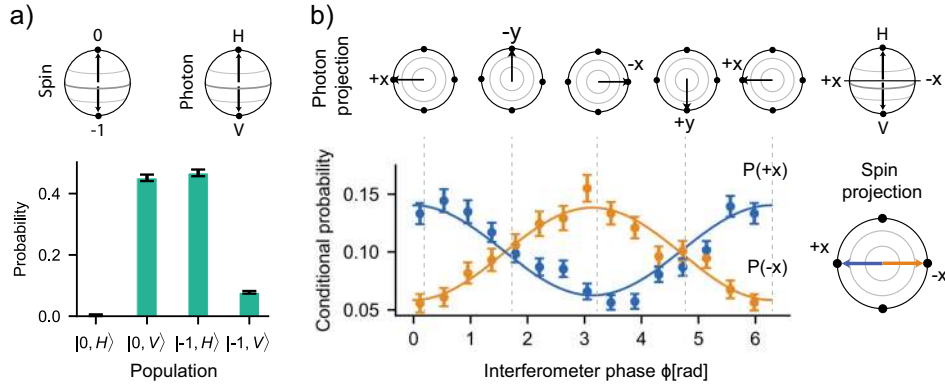
Fig. 4 Characterization of entanglement in orthogonal bases. a Measured correlations in the $\sigma_z \otimes \sigma_z$ basis. In the passive TPC scheme, photons which are generated in the first (second) excitation cycle and take the short (long) path enable direct projection in the $|0/-1\rangle$ and $|H/V\rangle$ (see methods). These photons enable the reconstruction of the diagonal density matrix elements of the spin-photon system. **b** Measured correlations in the $\sigma_x \otimes \sigma_x$ basis. Photons which arrive at the path-erasing time slot are expected to reveal a polarization correlation with the spin state in the equatorial bases. We plot the conditional probability of measuring the electron spin in the $|\pm x\rangle$ basis, upon detection of a ZPL photon, for a given interferometer phase ϕ, which sets the photon measurement basis to $|\phi\rangle = (|H\rangle + e^{i\phi}|V\rangle)/\sqrt{2}$. The blue (orange) points show the measurement data for preparation of the entangled states $|\psi\rangle = (|0\rangle|V\rangle \pm e^{i\phi}|-1\rangle|H\rangle)\sqrt{2}$, with corresponding sinusoidal fits (lines). The clear deviation from a flat line witnesses the entanglement generation. The phase uncertainty for each data point is ±0.18 radians, as determined from the resolution of the phase readout (see Supplementary Information). The error bars indicate the standard error of the mean.

additional laser and single-shot readout.[23,24] The spin mixing in the excited state can be removed almost entirely by using an NV in a low-strain environment.[17,24] High cooperativity cavity systems may even enable entangling schemes relying on single transitions without excitation of the emitter.[25,26]

Resolving these imperfections provides an imminent outlook for the scalability of the system. Particularly, seeing that NV centers, single atoms and molecules, or quantum dots are suited to the direct generation of two-dimensional cluster states using ancillary spins or remote centers,[11,12,18,27,28] the TPC scheme offers a robust and adaptable method to realize resource states for quantum communication and universal quantum computation.

METHODS

Sample and fabrication

An artificial, single-crystal diamond of natural isotopic abundance and with a {1, 1, 1} surface orientation hosts the NV center. We surveyed the diamond for shallow defects and created solid-immersion lenses using focussed ion-beam milling over several defects with the desired N-V axis orientation (perpendicular to the surface). We then coated the surface with 110 nm of SiO2 in order to reduce Fresnel reflection losses and laser backscatter at the high-index interface.

Experimental details

Our resonant optical pulses at around 637.2 nm are delivered from a narrowband external-cavity diode laser (Toptica DL Pro HP 637) and switched with two electro-optic amplitude modulators (Jenoptik AM635) in series. The fluorescence is split at a laser line filter into the resonant ZPL portion and the far off-resonant PSB portion. The latter was used to perform efficient spin readout. Since most (~ 97%) of the photons decay into the PSB[29] and the system has significant photon losses, the measured ZPL efficiency (pulse to click) is ~ 2×10^{-5}. The average probability of detecting a spin-readout click when prepared in $m_s = 0$ is (16.7 ± 0.1)%. We, therefore, observe an average of 25 PSB-ZPL coincidence events per hour.

The time-to-polarization conversion was performed by directing the ZPL part of the NV emission into a polarization-maintaining, fiber-based Mach-Zehnder interferometer. We matched the time between the two optical π-pulses in our sequence to the propagation delay between the arms of the interferometer. The interferometer was passively stabilized to minimize path length changes occurring during each entanglement cycle. The phase was furthermore tracked during each entanglement cycle by sending resonant laser pulses through the TPC between entanglement sequences

and measuring the intensity on four quadrature detectors corresponding to the photon states D, A, R, and L.

Passive routing of photons

The emitted photons are diagonally polarized with respect to the unbalanced interferometer's arms and therefore split in two possible propagation paths (50% take the H(V)-polarized long (short) arm) and two corresponding propagation times. Therefore, two excitation/emission cycles result in four arrival times at the output of the interferometer:

1. Early emission takes the short (V) path;
2. Early emission, long (H) path;
3. Late emission, short (V) path;
4. Late emission, long (H) path.

If the separation between the two emissions matches the time difference in the propagation, then events of type 2 and 3 have the same arrival time. Detection within this time window erases the path information and heralds the intended function of the passive switch (50% success probability). Events outside this window, 1 and 4, are path-revealing and are not conducive to the creation of the photonic polarization qubit.

Electron and nuclear spin initialization

The initialization sequence relies on electron and nuclear spin flips in the optically excited state of the NV center. A low-power laser pulse (5 μs long), resonant with the $0 \leftrightarrow 0_e$ transition, results in an electron (nuclear) spin flip with high (low) probability. Subsequently, nuclear spin selective microwave pulses are applied to the ground state, which drive the population in the undesired states back to 0. This sequence is repeated several times in order to enhance the probability of initializing the electron (nuclear) spin in state $|m_s = -1\rangle$ ($|m_I = 0\rangle$).

Fidelity estimation

Following a well-established method[21,28] we calculate the lower bound on the fidelity as:

$$F \geq 0.5 \left(\rho_{22} + \rho_{33} - 2\sqrt{\rho_{11}\rho_{44}} + C_{xx} \right) \qquad (1)$$

where ρ_{ii} denotes the diagonal entries of ρ and C_{xx} denotes the xx basis correlations $C_{xx} = \langle \sigma_x \otimes \sigma_x \rangle$ of ρ. The diagonal elements $\rho_{11}, ..., \rho_{44}$ are directly extracted from the data in Fig. 4a, whereas the equatorial correlations C_{xx} are calculated from the contrast of the curves in Fig. 4b.

Further details of all methods are provided in the Supplementary Information.

Note: During preparation of the manuscript, we became aware of preliminary efforts towards the results achieved in this work using a

quantum dot.[30] During the review process of this article, an implementation of the scheme combined with photon frequency conversion was published.[31]

DATA AVAILABILITY

The data supporting the findings of this work are available from the corresponding author, upon reasonable request.

REFERENCES

1. Ladd, T. D. et al. Quantum computers. *Nature* **464**, 45–53 (2010).
2. Rudolph, T. Why I am optimistic about the silicon-photonic route to quantum computing. *APL Photon.* **2**, 030901 (2017).
3. Gisin, N. & Thew, R. Quantum communication. *Nat. Photon.* **1**, 165–171 (2007).
4. Buterakos, D., Barnes, E. & Economou, S. E. Deterministic generation of all-photonic quantum repeaters from solid-state emitters. *Phys. Rev. X* **7**, 041023 (2017).
5. Degen, C., Reinhard, F. & Cappellaro, P. Quantum sensing. *Rev. Modern Phys.* **89**, 035002 (2017).
6. Kwiat, P. G. et al. New high-intensity source of polarization-entangled photon Pairs. *Phys. Rev. Lett.* **75**, 4337–4341 (1995).
7. Briegel, H. J. & Raussendorf, R. Persistent entanglement in arrays of interacting particles. *Phys. Rev. Lett.* **86**, 910–913 (2001).
8. Briegel, H. J., Browne, D. E., Dür, W., Raussendorf, R. & Van den Nest, M. Measurement-based quantum computation. *Nat. Phys.* **5**, 19–26 (2009).
9. Walther, P. et al. Experimental one-way quantum computing. *Nature* **434**, 169–176 (2005).
10. Lindner, N. & Rudolph, T. Proposal for pulsed on-demand sources of photonic cluster state strings. *Phys. Rev. Lett.* **103**, 113602 (2009).
11. Russo, A., Barnes, E. & Economou, S. E. Photonic graph state generation from quantum dots and color centers for quantum communications. *Phys. Rev. B* **98**, 085303 (2018).
12. Economou, S. E., Lindner, N. & Rudolph, T. Optically generated 2-dimensional photonic cluster state from coupled quantum dots. *Phys. Rev. Lett.* **105**, 9 (2010).
13. Schwartz, I. et al. Deterministic generation of a cluster state of entangled photons. *Science* **354**, 434–437 (2016).
14. Doherty, M. W. et al. The nitrogen-vacancy colour centre in diamond. *Phys. Rep.* **528**, 1–45 (2013).
15. Nemoto, K. et al. Photonic architecture for scalable quantum information processing in diamond. *Phys. Rev. X* **4**, 031022 (2014).
16. Togan, E. et al. Quantum entanglement between an optical photon and a solid-state spin qubit. *Nature* **466**, 730–734 (2010).
17. Goldman, M. L. et al. Phonon-induced population dynamics and intersystem crossing in nitrogen-vacancy centers. *Phys. Rev. Lett.* **2**, 1–7 (2014).
18. Rao, D. D. B., Yang, S. & Wrachtrup, J. Generation of entangled photon strings using NV centers in diamond. *Phys. Rev. B* **92**, 081301 (2015).
19. Aharonovich, I., Englund, D. & Toth, M. Solid-state single-photon emitters. *Nat. Photon.* **10**, 631–641 (2016).
20. Awschalom, D. D., Hanson, R., Wrachtrup, J. & Zhou, B. B. Quantum technologies with optically interfaced solid-state spins. *Nat. Photon.* **12**, 516 (2018).
21. Blinov, B. B., Moehring, D. L., Duan, L.-M. & Monroe, C. Observation of entanglement between a single trapped atom and a single photon. *Nature* **428**, 153–157 (2004).
22. Riedel, D. et al. Deterministic enhancement of coherent photon generation from a nitrogen-vacancy center in ultrapure diamond. *Phys. Rev, X* **7**, 031040 (2017).
23. Yang, S. et al. High-fidelity transfer and storage of photon states in a single nuclear spin. *Nat. Photon.* **10**, 507–511 (2016).
24. Robledo, L. et al. High-fidelity projective read-out of a solid-state spin quantum register. *Nature* **477**, 574–578 (2011).
25. Sun, S. & Waks, E. Deterministic generation of entanglement between a quantum-dot spin and a photon. *Phys. Rev. A* **90**, 042322 (2014).
26. Sun, S., Kim, H., Solomon, G. S. & Waks, E. A quantum phase switch between a single solid-state spin and a photon. *Nat. Nanotechnol.* **11**, 539–544 (2016).
27. Fuchs, G. D., Burkard, G., Klimov, P. V. & Awschalom, D. D. A quantum memory intrinsic to single nitrogen-vacancy centres in diamond. *Nat. Phys.* **7**, 789–793 (2011).
28. Bernien, H. et al. Heralded entanglement between solid-state qubits separated by three metres. *Nature* **497**, 86–90 (2013).
29. Jelezko, F. & Wrachtrup, J. Single defect centres in diamond: a review. *Phys. Status Solidi (a)* **203**, 3207–3225 (2006).
30. Lee, J. P. et al. A quantum dot as a source of time-bin entangled multi-photon states. *Quant. Sci. Technol.* **4**, 025011 (2019).
31. Tchebotareva, A. et al. Entanglement between a diamond spin qubit and a photonic time-bin qubit at telecom wavelength. *Phys. Rev. Lett.* **123**, 063601 (2019).

AUTHOR CONTRIBUTIONS

R.V., S.R., and C.S. contributed equally to this work. R.V., S.R., and C.S. performed the experiments. R.V., S.R., C.S., and M.T. analyzed the data. G.W. and D.W. contributed to the experimental apparatus. J.S., P.W., and M.T. provided support for the work. M.T. devised the scheme, supervised the work, and drafted the manuscript. All authors contributed to the interpretation of the data and the writing of the manuscript.

COMPETING INTERESTS

The authors declare no competing interests.

ADDITIONAL INFORMATION

Supplementary information is available for this paper at https://doi.org/10.1038/s41534-019-0236-x.

Correspondence and requests for materials should be addressed to M.T.

Reprints and permission information is available at http://www.nature.com/reprints

Publisher's note Springer Nature remains neutral with regard to jurisdictional claims in published maps and institutional affiliations.